

Article

Biogeochemical Redox Processes Controlling the Element Cycling: Insights from Karst-Type Bauxite, Greece

Maria Economou-Eliopoulos ^{1,*} , Marioka Kontou ² and Ifigeneia Megremi ¹

¹ Department of Geology and Geoenvironment, National University of Athens, GR-15784 Athens, Greece; megremi@geol.uoa.gr

² 1st High School of Kallipolis, GR-18538 Athens, Greece; mrsineti@gmail.com

* Correspondence: econom@geol.uoa.gr

Abstract: The occurrence of very-high-grade bauxite ores of karst-type deposits resulting from Fe-leaching is of particular importance, because they are widespread in the Mediterranean metallogenetic province and result in the natural beneficiation of the ore quality. The present study focuses on mineral transformations and variations of major and trace elements, including platinum-group elements (PGE) and mineral chemistry along a bauxite profile from the Parnassos-Ghiona deposit, Greece underlying a fault. The most salient feature of the multicolor ores (grey–whitish, yellowish, deep red, deep grey to brown-red color, from top to bottom) is their association with fossilized and present-day microorganisms, which, by their reducing and/or oxidizing activity, catalyze redox reactions and provide nucleation sites for the precipitation of secondary minerals. Texture relationships between mineral and variations in the mineral chemistry, suggesting the sequence in their formation, indicate a multistage evolution. The recorded compositional variations show that the Al enrichment is accompanied by increase in the TOC, As, Pd and U, and chondrite-normalized REE patterns exhibit a similar trend and positive Ce anomalies. A lower (Pt + Pd) content and higher Pd/Pt ratio, ranging from 1.0 to 5.5 in the bauxite profile compared to those in Fe-Ni laterite deposits with the Pd/Pt ratio ranging from 0.1 to 0.68, reflect the higher solubility and mobility of Pd compared to that of Pt, and differences in their origin and genesis. A positive correlation between Pd and As and the elevated As content (up to 960 mg/kg) in multicolor ores compared to brown-red samples (average 10 mg/kg As) confirms their mobilization and redeposition.

Keywords: bauxite; biogeochemical; microorganism; ore-beneficiation



Citation: Economou-Eliopoulos, M.; Kontou, M.; Megremi, I. Biogeochemical Redox Processes Controlling the Element Cycling: Insights from Karst-Type Bauxite, Greece. *Minerals* **2022**, *12*, 446.

<https://doi.org/10.3390/min12040446>

Academic Editor: Tiago Osorio Ferreira

Received: 22 February 2022

Accepted: 1 April 2022

Published: 5 April 2022

Publisher's Note: MDPI stays neutral with regard to jurisdictional claims in published maps and institutional affiliations.



Copyright: © 2022 by the authors. Licensee MDPI, Basel, Switzerland. This article is an open access article distributed under the terms and conditions of the Creative Commons Attribution (CC BY) license (<https://creativecommons.org/licenses/by/4.0/>).

1. Introduction

The role of microorganisms in transforming organic and inorganic substrates is of particular significance in geology, mineralogy, and biogeochemical cycles of metals/metalloids [1]. Some of the activities of microorganisms in biogeochemical processes resulting in metal distributions and speciation may take place in aquatic and terrestrial ecosystems and are mainly related to physicochemical parameters. Many minerals are of biogenic origin and provide evidence for the role of microorganisms in geological processes [1–4]. Specially, uptake, assimilation, degradation and metabolism of organic and inorganic compounds, respiration (CO₂ production), photosynthesis, biosynthesis of polymers, and humus formation are a few representative examples showing the role of microorganisms in elemental cycles [1]. Natural weathering of rocks and ores/mining and/or smelting wastes, industrial and urban waste leachates, and agricultural activities are common sources of contamination for the soil-groundwater-plant/crop system [5,6]. On the other hand, bioremediation has been used to remove harmful elements from contaminated soil and groundwater, and applications of microorganisms as a green alternative process to the metal recovery have been widely recommended, due to high capital and energy costs of the very expensive involved techniques to reduce contamination of degraded ecosystems and pyrometallurgical techniques [7–9].

Among large deposits of economic significance is bauxite, the source for the recovery of aluminum. Weathering of source rock is promoted by the activities of microorganisms mobilizing Al, Fe, and Si, which subsequently precipitate as oxides, silica, and silicate minerals [4]. The presence of organic matter, in the form of fossilized matter and/or thin coal layers locally overlaying bauxite, is a common feature above bauxite deposits. The occurrence of very-high-grade bauxite deposits of karst-type, resulting from Fe-leaching during or after bauxite formation, is well known in the Mediterranean metallogenetic province, including the Parnassos-Ghiona Mountains (Greece) [10–14], Southern France and Spain [15], Montenegro (Dinarides) [16], Hungary, Croatia, Turkey (Doğankuzu and Mortas, Taurides), and elsewhere [15,17]. The present study focuses on mineral transformations and variations of the bulk (major and trace elements, including platinum-group elements) and mineral chemistry along a bauxite profile from the Parnassos-Ghiona deposit, Greece (approximately two meters thickness), underlying a fault. A consortium of fossil bacteria and biominerals were identified within that transitional zone of varying color (top to bottom) from grey-whitish, yellowish, deep red, deep grey to brown-red color. The mineralogical and biogeochemical features of such transitional zones are of particular importance because they are widespread along highly faulted zones throughout karst-type bauxite deposits, resulting in beneficiation of ore quality and ore exploration.

2. Materials and Methods

Morphological and geochemical characteristic have been described in previous studies [10,11,18,19]. Fourteen bauxite samples along a profile (~2 m) underlying a fault from the B₃ formation of the Parnassos-Ghiona deposit (Figure 1) were chosen for this study to be representative of all multicolor ore types. Due to the heterogeneous character of the bauxite deposit, samples of approximately 2 kg weight were collected. They were prepared and analyzed for major and trace elements, including rare-earth elements (REE) by inductively coupled plasma mass spectrometry (ICP-MS) analysis, after multi-acid digestion (HNO₃–HClO₄–HF–HCl) at the ACME Laboratories Ltd., Vancouver, BC, Canada (Table 1). Detection limits, quality control samples and the precision of the analyses are in agreement with international standards (~10%). The platinum-group elements (PGE) analyses were obtained using lead collection fire-assay preconcentration technique from large (25 g) samples at Genalysis Laboratory Services, Perth, Australia. This method allows for complete dissolution of samples. The detection limits were 0.5 µg/kg for Pd, 0.1 µg/kg for Pt, and 1.0 µg/kg for Au. Sulfur was determined at the Technical University of Athens using a LECO instrument, and total organic carbon at the Athens University, following the titration method of [20].

The SEM-EDS backscattered electron images and analyses were carried out at the Faculty of Geology and Geoenvironment, National and Kapodistrian University of Athens (NKUA), using a JSM-5600 (JEOL, Tokyo, Japan), scanning electron microscope, equipped with ISIS 300 (Oxford Instruments, Abingdon, UK), automated energy dispersive analysis system. Analytical conditions were 20 kV accelerating voltage, 0.5 nA beam current, <2 µm beam diameter, and 50 s count times. The following X-ray lines were used: FeK α , NiK α , CoK α , CuK α , CrK α , AlK α , TiK α , CaK α , SiK α , MnK α and MgK α ; Cr, Fe, Mn, Ni, Co, Ti, and Si; MgO for Mg; and Al₂O₃ for Al.

Batch-leaching experiments were carried out, 20 g of a crushed ore and red mud (metallurgical residue slag) and 150 mL of natural water in a 200 mL Erlenmeyer flask, at room temperature. The reaction flask was shaken at approximately 120 rpm by a reciprocal shaker for one week. After the period of shaking, the slurries were filtered through a 0.45 µm polyamide membrane filter. The filtered leachates were analyzed by inductively coupled plasma mass spectroscopy (ICP-MS) at ACME Analytical Laboratories in Canada.

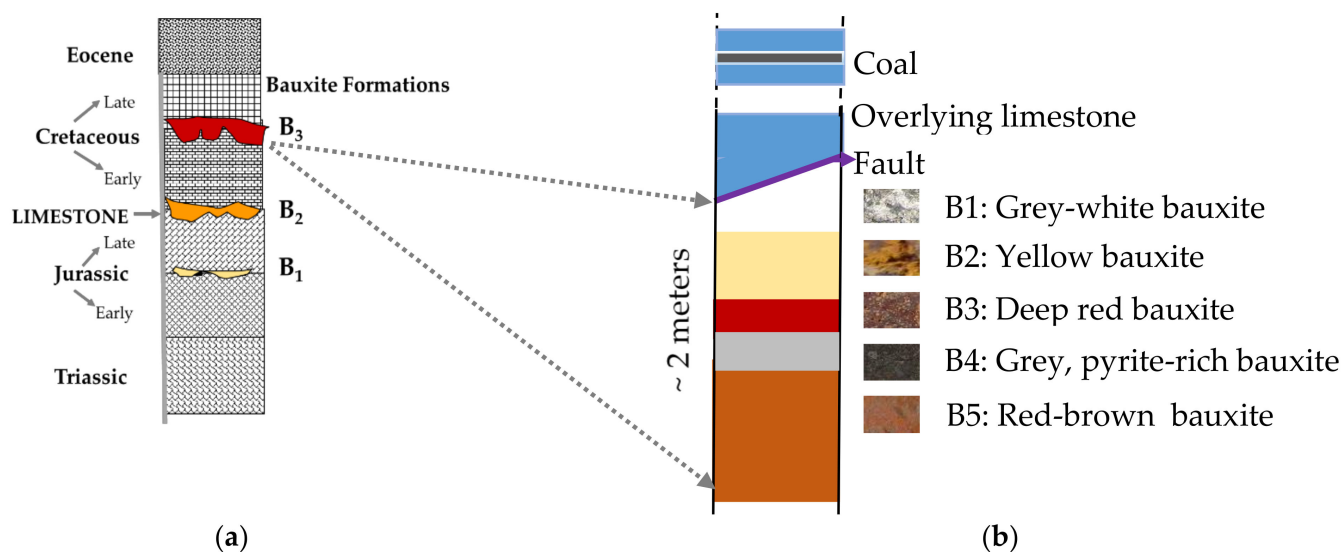


Figure 1. Stratigraphic column of the Parnassos-Ghiona bauxite deposits, showing the bauxite formations in relation to the age on the associated limestones (a) and the brief sequence of the studied bauxite types, along a profile from B₃ formation, although there is commonly coexistence on yellow, grey, and deep red bauxite, in a varying proportion (b).

Table 1. Major and trace element content in bauxite from the Parnassos-Ghiona deposit, along a profile underlying a fault (Figure 1).

	Grey-Whitish			White-Yellow				Deep Red	Deep Grey			Brown-Red		
Samples	B1.1	B1.2	B1.3	B2.1	B2.2	B2.3	B2.4	B3	B4.1	B4.2	B4.3	B5.1	B5.2	B5.3
mg/kg														
As	25	78	17	540	240	220	960	380	520	220	34	7.2	16	8
Co	16	6	16	11	12	7	16	10	61	47	36	20	29	9
Cr	1230	1000	980	1140	3280	1140	1100	940	960	990	980	1230	1220	1140
Hf	18	16	13	14	17	17	15	16	12	13	13	15	14	16
Sc	61	36	66	51	55	53	33	57	37	46	54	44	77	60
Sb	14	7.8	1.7	28	25	25	21	8.4	25	16	5.4	1.3	4.9	1.5
Ta	5.4	5	4.8	3.6	5.3	4.7	2.8	3.6	3.5	3.7	4.7	4.9	5.9	4.9
Th	31	45	53	34	36	28	59	45	42	49	47	54	58	50
U	5.5	5.2	5.6	5.8	4.5	5.7	6.5	6.4	8.2	6.3	4.5	6.4	6.1	4.8
La	13	15	9	27	30	25	17	21	33	16	7	23	25	26
Ce	110	95	130	100	80	170	96	76	83	42	120	130	140	120
Sm	1.7	2.9	2.2	1.8	2.7	2.6	3.4	3.5	3.2	4.1	2.2	3.8	5.8	2.7
Eu	0.4	0.6	0.5	0.6	0.6	0.5	0.7	0.7	0.8	0.9	0.4	0.9	1	0.5
Yb	5.9	6.9	4.5	6.9	9.2	5.3	6.6	8.4	5.3	6.9	3.8	8.5	8.4	8.1
Lu	0.9	1.1	0.7	1	1.6	0.8	1	1.3	0.9	1.1	0.6	1.4	1.4	1.3
µg/kg														
Au	80	26	89	26	35	7	88	5	40	37	50	28	24	42
Pt	0.8	<0.1	0.4	0.6	<0.1	0.5	0.4	1.9	<0.1	0.8	<0.1	0.1	0.4	0.4
Pd	2.6	1.8	0.5	3	1.7	0.5	2.2	2	1.6	2.1	0.7	1.3	<0.5	0.8
wt. %														
Al ₂ O ₃	69.1	58.1	55.8	58.6	59.9	63.7	63.7	49.9	65.3	52	51	56.9	50.6	48
FeO	0.56	0.31	6.9	0.22	0.52	0.3	0.17	0.45	2.5	26.42	3.1	2.21	2.12	1.79
S	0.26	0.15	0.36	0.19	0.17	0.2	0.17	0.16	10.64	8.4	4.02	0.16	0.15	0.17
TOC	2.28	2.06	2.73	2.23	1.67	1.68	2.56	2.21	5.4	1.8	2.98	0.08	0.19	0.26

3. Geological Outline

The Parnassos-Ghiona bauxite deposits of Greece are part of the Mediterranean karst bauxite belt. These deposits are hosted within carbonate rocks and have different ages. Three bauxite formations, B₁, B₂, and B₃, from the oldest to the youngest, can be distinguished (Figure 1), and are intercalated with shallow water limestone within a Late Jurassic to Cretaceous sequence of the Parnassos-Ghiona zone [21] (Figure 1). The organic matter, as thin coal layers, overlying the bauxite deposits has been described [13]. Intense tectonism has affected those bauxite deposits, producing overthrusting, faulting, and disruption of the continuity of the bauxite bodies [21], facilitating the meteoric fluid circulation and mineral deposition. The studied profile belongs to the B₃ formation (or horizon), hosting both high-Fe and high-Al bauxite ores, under exploitation. The significant proportion (approximately 30% volume) of transformed bauxite ore, similar to that of the studied profile (Figure 1), is the most characteristic feature. Specifically, at the Pera-Lakkos bauxite deposit, grey to whitish–grey bauxite gradually grades downwards through yellow, deep red, and deep grey to brown-red-colored bauxite ore (Figure 1).

4. Mineralogical Characteristics

The main mineralogical characteristics of the Parnassos-Ghiona bauxite deposits have been described by previous authors [10–14,21,22]. Typical bauxite ore is dominated by pelitomorphic (fine-grained), ooidic-pisolitic and clastic texture, and by dark red to red-brown color. The AlOOH polymorphs boehmite and diaspore, forming pisoliths and oolites, are the main components of the Parnassos-Ghiona bauxite ores, while gibbsite (Al₂O₃·3H₂O), goethite and/or hematite are present in lesser amounts. Kaolinite, illite and pyrite are common in thrust-fault-affected parts of the deposits, whereas chamosite, quartz and zircon are present in lesser amounts. The present study is focused on bauxite samples affected by the presence of microorganisms (Figure 2). Bauxite ores from the transition zone of the from the Parnassos-Ghiona bauxite deposit show whitish-grey, yellow, deep red color (Figure 2a), and red to deep grey for the sulfide-rich ore (Figure 2b). Thin sulfide veins may crosscut earlier-transformed grey bauxite ore, including goethite and/or occur as remnants in neoformed goethite (Figure 2d–e).

Fossilized microorganisms of different morphological forms are revealed in unpolished parts of the polished bauxite sections (Figure 2f–h). Goethite microtextures resembling a variety of fossilized microorganisms coated by goethite (white arrows), including filament-like, rods, and coccus-type forms, of various sizes are present in multicolor bauxite samples, mostly in close association with sulfides and Fe-oxides (Figure 2f–h). Fine pyrite and large clusters of framboidal pyrite showing textural evidence of bacteria replacement (Figure 2i) are common. In addition, a salient feature of bauxite samples from the studied transitional zone is the formation of new minerals on hand samples (Figure 2j) and polished sections (Figure 2k), which are covered by a whitish soft mass, under normal atmospheric conditions in a few months. These present-day neoformed minerals are mainly hydrated Al- and Fe-sulfates, under a needle-like morphology such as halotrichite [Fe²⁺Al₂(SO₄)₄·22(H₂O)], and fine-grained voltaite [K₂Fe²⁺5Fe³⁺ 3Al(SO₄)₁₂·18(H₂O)] and szomolnokite [(Fe²⁺SO₄·(H₂O))] (Figure 2k–m) [19].

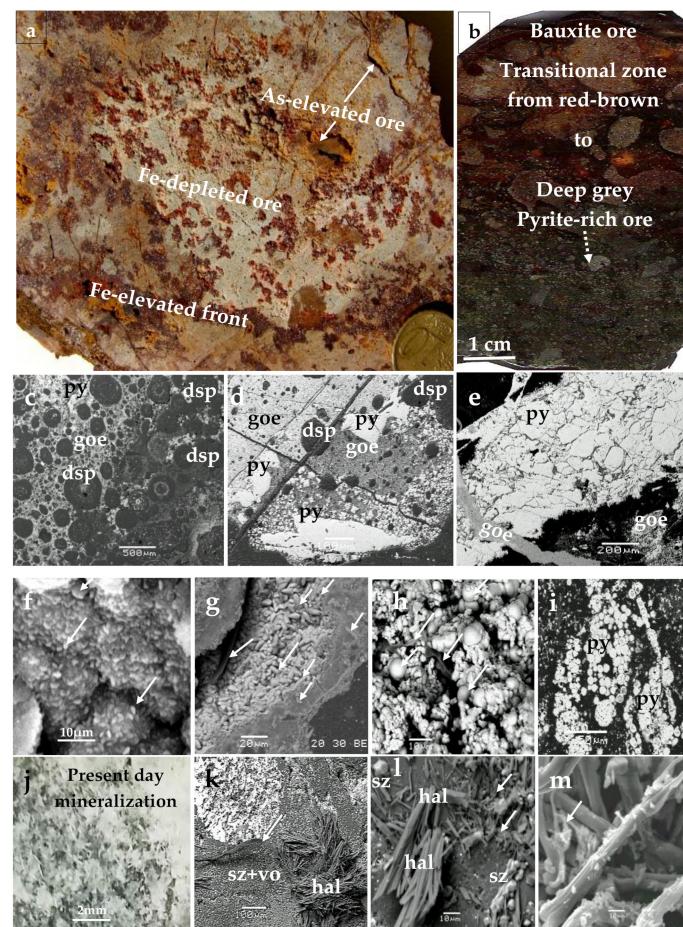


Figure 2. Photographs of hand bauxite samples from the transition zone of whitish-grey, yellow and deep red color (a) and a transformed red to deep grey sulfide-rich ore from the Parnassos-Ghiona bauxite deposit (b). Backscattered electron images (BSE) of grey-red bauxites showing pisoliths and matrix dominated by diaspore (c), the association of pyrite remnants with goethite (d), vein of pyrite crosscutting goethite and goethite vein crosscutting pyrite (e). The unpolished parts of the bauxite sample revealed the presence of goethite microtextures resembling variety of fossilized microorganisms coated by goethite (white arrows) (f–i); replacement of fine-grained framboidal pyrite by a coarser-grained pyrite and the coexistence of pyrite, either as fine-grained spherical pyrite and pyrite pseudomorphs (h). Present-day biomineralization on hand bauxite sample (j); BSE images of aggregates of hydrous sulfate minerals: halotrichite, szomolnokite, and voltaite (k–m) from polished sections. Abbreviations: py = pyrite; goe = goethite; dsp = diaspore; hal = halotrichite; sz = szomolnokite.

5. Geochemical Characteristics

5.1. Bauxite Ores

The most salient feature in the geochemical composition of the Parnassos-Ghiona bauxite deposit is a wide variation occurring along and near faults of the deposit. Arsenic ranges from 7.2 to 16 mg/kg in the typical brown-red-colored ore and from 34 to 960 mg/kg in yellow-, deep red-, and deep grey-colored ore (average 390 mg/kg), while in whitish ore it ranges from 17 to 76 mg/kg (Table 1). The multicolor bauxite ore is characterized by elevated total organic carbon (TOC) content (up to 5.4 wt.%) compared to the brown-red ore (0.08–0.26 wt.%). In addition, 0.66 wt.% O.M. was determined in a whitish material grown after a few weeks on the surface of grey bauxite samples, exposed to air oxidation, in the room conditions (20–25 °C) and moderate air humidity (atmospheric water). The main components of that epigenetic material are hydrated Al- and Fe-sulfates (Figure 2j–l) which are similar to those identified on polished and unpolished sections [19]. The highest S and

FeO contents occur in the samples with deep grey color, reaching values up to 10.8 wt.% S and 26.4 wt.% FeO (Table 1), which are consistent with the presence of abundant pyrite (Figure 2). The lowest contents of REE were recorded in a sulfide-rich bauxite sample (Table 1).

Based on the presented analytical data (Table 1), the calculated correlation matrix (Table 2) shows positive values (≥ 0.5) between TOC and Al, As, Sb, S, and Co, and negative values with Yb, Lu, and Ta. Also, Pd increases with increasing As content (Figure 3a) and decreases with the increasing Ce and Sc contents (Figure 3b,c). Scandium shows a negative correlation with As (Figure 3d).

Table 2. Correlation matrix of major and trace elements in bauxites from a transitional zone of the Parnassos-Ghiona bauxite deposit. Data from Table 1.

	As	Co	Cr	Hf	Sc	Sb	Ta	Th	U	La	Ce	Sm	Eu	Yb	Lu	Au	Pt	Pd	Al ₂ O ₃	FeO	S	TOC	
As	1.00																						
Co	0.09	1.00																					
Cr	−0.03	−0.22	1.00																				
Hf	−0.14	−0.74	0.40	1.00																			
Sc	−0.58	−0.18	0.12	0.11	1.00																		
Sb	0.67	0.11	0.33	0.08	−0.39	1.00																	
Ta	−0.85	−0.25	0.34	0.37	0.64	−0.45	1.00																
Th	0.02	0.21	−0.28	−0.47	0.00	−0.61	−0.09	1.00															
U	0.50	0.57	−0.41	−0.45	−0.37	0.26	−0.55	0.18	1.00														
La	0.28	0.07	0.39	0.09	−0.08	0.49	−0.08	−0.24	0.36	1.00													
Ce	−0.37	−0.37	−0.14	0.20	0.41	−0.26	0.50	−0.05	−0.23	−0.04	1.00												
Sm	−0.02	0.33	−0.07	−0.25	0.14	−0.25	0.09	0.62	0.39	0.25	−0.07	1.00											
Eu	0.16	0.44	−0.06	−0.39	−0.11	−0.03	−0.14	0.52	0.62	0.40	−0.27	0.89	1.00										
Yb	−0.01	−0.31	0.48	0.39	0.11	−0.07	0.17	0.17	−0.04	0.54	−0.24	0.49	0.51	1.00									
Lu	−0.07	−0.22	0.56	0.35	0.12	−0.09	0.25	0.19	−0.05	0.56	−0.24	0.52	0.53	0.98	1.00								
Au	0.13	0.08	−0.06	−0.13	−0.02	−0.11	−0.08	0.28	−0.06	−0.53	−0.03	−0.33	−0.33	−0.44	−0.42	1.00							
Pt	0.16	−0.21	−0.27	0.23	0.26	−0.03	−0.31	−0.11	0.17	−0.08	−0.27	0.07	0.04	0.21	0.09	−0.22	1.00						
Pd	0.53	−0.07	0.06	0.19	−0.49	0.51	−0.53	−0.35	0.19	0.06	−0.66	−0.35	−0.05	0.15	0.06	0.11	0.32	1.00					
Al ₂ O ₃	0.37	0.00	0.15	0.29	−0.40	0.63	−0.13	−0.52	0.29	0.13	0.07	−0.40	−0.22	−0.29	−0.29	0.33	−0.22	0.41	1.00				
FeO	−0.12	0.52	−0.17	−0.45	−0.05	−0.06	−0.19	0.22	0.14	−0.26	−0.50	0.27	0.35	−0.10	−0.08	0.07	0.13	0.05	−0.30	1.00			
S	0.16	0.93	−0.22	−0.66	−0.36	0.26	−0.40	0.02	0.54	0.11	−0.50	0.14	0.30	−0.36	−0.28	0.00	−0.14	0.08	0.06	0.58	1.00		
TOC	0.46	0.51	−0.18	−0.42	−0.42	0.46	−0.52	−0.25	0.44	−0.06	−0.34	−0.38	−0.22	−0.64	−0.60	0.28	−0.06	0.28	0.46	0.00	0.62	1.00	

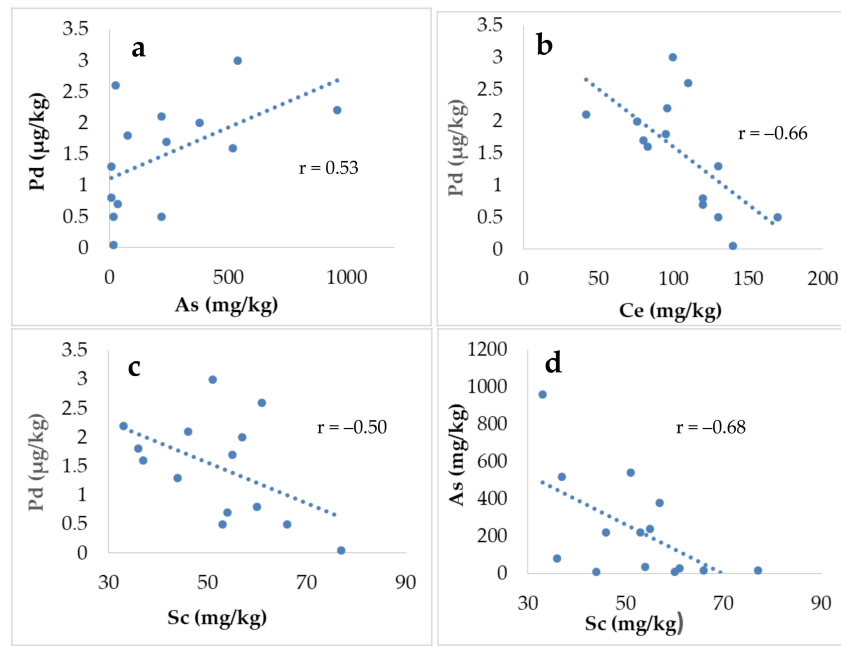


Figure 3. Plots of Pd versus As, Ce, and Sc (a–c), and As versus Sc (d) from the bauxite profile (Figure 1). Data are from Table 1.

The schematic compositional variations present the Al enrichment, accompanied by REE, As, Pd, U, and TOC in the transformed multicolor ores compared to brown-red bauxite ores, and a very good correlation ($r = 0.89$) between Sm and Eu (Table 2; Figures 4 and 5).

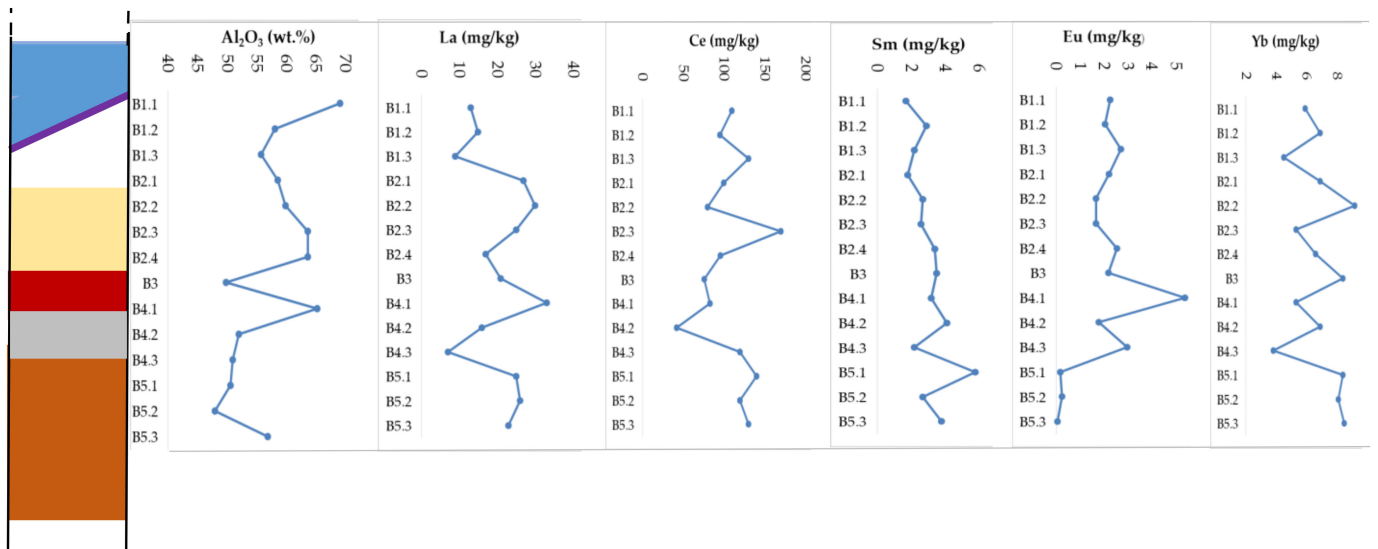


Figure 4. Schematic compositional variations for Al_2O_3 , La, Ce, Sm, Eu, and Yb (similar to the variation for Lu), through a vertical bauxite profile (Figure 1). Data are from Table 1.

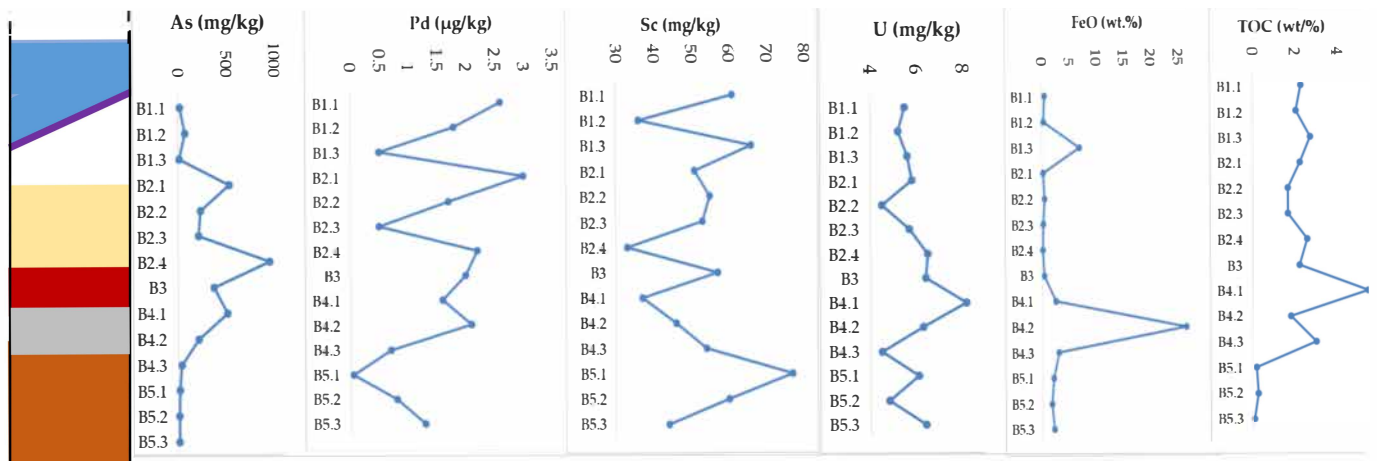


Figure 5. Schematic compositional variations for As, Pd, Sc, U, FeO, and TOC, through a vertical bauxite profile (Figure 1). Data are from Table 1.

Palladium shows positive correlation with As and Sb and negative with Ce (Figure 5). The correlations between S and FeO, Co, and U are positive, as well as the interelement correlation between heavy rare-earth elements (HREE). It is obvious that a very good positive correlation between S and Co ($r = 0.93$) reflects the association of Co with sulfides. Scandium content varies from 33 to 77 mg/kg (average 53 mg/kg), with the highest content in a sample of brown-red color (Table 1) and it shows a negative correlation with As and Pd (Figure 3c,d).

The chondrite-normalized REE patterns for bauxite samples from the studied profile of the Parnassos-Ghiona bauxite exhibit a similar trend to those analyzed and presented for the total of REE [11], showing positive Ce anomalies for all samples, although the anomaly is greater compared to sulfide-rich samples. The LREE enrichment compared to HREE is obvious (Figure 6).

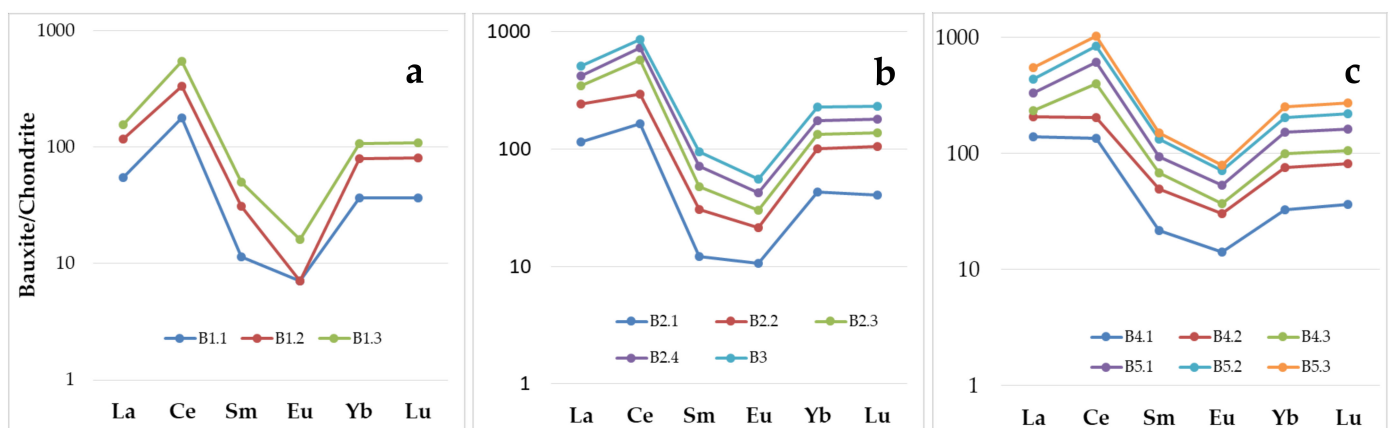


Figure 6. Chondrite-normalized REE patterns for bauxite samples from the Parnassos-Ghiona of varying color (a): Grey-whitish; (b): yellow and deep red; (c): deep grey and brown-red. Data are from Table 1.

5.2. Water Leachates of Bauxite Ore and Red Mud

Since the mining and smelting processes are potential sources of contamination and can be a threat for the environment, water leachates from representative samples of bauxite ore from the studied profile and bauxite-processing residue or red mud from the Aspra Spitia plant, Greece (May 2008), are given as well (Table 3). These leachates show relatively elevated concentrations of Zn, Co, Cr, Mn, Ni, Cu, U, Ca, Mg, Na, K, and S. In particular,

very high Cr(VI) concentrations exhibit the water leachate from the red mud. The concentrations for all REE, PGE, and As in both water leachates are lower than the detection limit of the method (Table 3).

Table 3. Trace element concentration in water leachates from bauxite (B5.2) and red mud (L.R.mud) [23] samples.

$\mu\text{g/L}$	B5.2	L.R.mud	Detection	$\mu\text{g/L}$	B5.2	L.R.mud	Detection
1-8	30	13,700	1	V	0.4	6160	0.2
Al	<0.5	280	0.5	W	110	1290	0.02
As	<0.05	<0.05	0.05	Y	0.02	<0.01	0.01
Cd	0.22	1	0.02	Zn	7.8	1.0	0.5
Co	2.1	2200	0.5	Zr	<0.02	<0.02	0.02
Cr	1.1	2100	0.5	La	<0.01	<0.01	0.01
Cr(VI)	0.6	5	0.1	Ce	<0.01	<0.01	0.01
Cu	<10	<10	10	Pr	<0.01	<0.01	0.01
Fe	0.08	90	0.05	Nd	<0.01	<0.01	0.01
Ga	<0.05	<0.05	0.05	Sm	<0.02	<0.02	0.02
Ge	<0.1	<0.1	0.1	Eu	<0.01	<0.01	0.01
Hg	<0.01	<0.01	0.01	Gd	<0.01	<0.01	0.01
In	1.5	7	0.1	Tb	<0.01	<0.01	0.01
Li	0.99	<0.05	0.05	Dy	<0.01	<0.01	0.01
Mn	4.6	740	0.1	Ho	<0.01	<0.01	0.01
Mo	<0.01	<0.01	0.01	Er	<0.01	<0.01	0.01
Nb	2.4	0	0.2	Tm	<0.01	<0.01	0.01
Ni	<10	15	10	Yb	<0.01	<0.01	0.01
P	62	<0.1	0.1	Lu	<0.01	<0.01	0.01
Pb	0.45	19	0.01	Ru	<0.05	<0.05	0.05
Rb	0.04	0.12	0.01	Rh	<0.01	<0.01	0.01
Re	2.13	2.2	0.05	Pt	<0.01	0.06	0.01
Sb	<1	<1	1	Pd	<0.2	<0.2	0.2
Sc	7.3	110	0.5	Au	<0.05	<0.05	0.05
Se	3190	430	40				
Si	140	0.05	0.01	mg/L			
Sr	<0.02	<0.02	0.02	Ca	61	0.32	0.05
Ta	<0.05	<0.05	0.05	Mg	1.6	0.08	0.05
Te	<10	<10	10	Na	15	310	0.05
Th	0.07	<0.01	0.01	K	0.6	11	0.05
Tl	1.34	<0.02	0.02	Cl	13	38	1
U				S	13	65	1

6. Discussion

Microorganisms are considered as a key controlling factor for mineral transformation, the metal/metalloid mobilization, enrichment, and biomineralization in the Earth system [1,4,24–28]. A consortium of microorganisms of varying morphological forms may produce enzymes and catalyze redox reactions and provide nucleation sites for the precipitation of secondary minerals [24,29,30]. The mineralogical and biogeochemical features reflecting the interaction with microorganisms at highly faulted zones throughout Parnassos-Ghiona bauxite deposits have been described in detail [10–14,18,22]. The spatial association of microorganisms and main minerals in the bauxite deposits, the described bacteriomorphic goethite and pyrite, and the negative $\delta^{34}\text{S}$ values for sulfide-bearing samples point to the existence of the appropriate conditions for iron bioleaching, Al enrichment, and biomineralization [10,11]. In addition, Cretaceous white bauxite of high quality is the type of the economic importance in the Montenegro (Bijele Poljane) bauxite deposits [16], Cretaceous bauxites in Serbia [31], Cretaceous reddish, yellowish, and greyish bauxites at Ayranci, Karaman, and Turkey [32], Late Permian grey bauxites at the Kanirash deposit, NW Iran [17], and elsewhere, suggesting an important role of microorganisms to biogeochemical processes.

6.1. Biogeochemical Cycling of Metals/Metalloids in a Bauxite Profile

The investigation of bauxite samples along a profile (Figures 1–6, Tables 1–3) provides an approach in understanding the consequence of the biogeochemical processes during the bauxite formation, diagenesis/meta-diagenesis stages, the compositional variations along the profile, and relationships between redox-sensitive elements and TOC. Considering the transformation process of the bauxite, it seems likely that the interaction of Al-Fe-oxides with reducing microorganisms results in the Fe(III) reduction to soluble Fe(II), and, in

turn, the Al, REE, and As enrichment (Figure 2a,b). Subsequently, part of the mobilized Fe(II) may be reprecipitated mainly as pyrite (Figure 2c,d), followed by the activity of oxidizing microorganisms and the replacement of pyrite by goethite and/or hematite (Figure 2d,e). Thus, under the activity of reducing microorganisms, Fe(II) may migrate, and fine-grained framboidal pyrite is present as veins crosscutting previous phases (Figure 2i). In addition, veinlets of goethite crosscutting all previous minerals (Figure 2e) reflect the multistage formation of minerals at a wide range of Eh-pH conditions during diagenetic and epigenetic stages. The higher As contents in the multicolor, compared to brown-red, bauxite samples (Table 1; Figure 5) may be the result of mobilization and redeposition, while the negative correlation with less mobile elements, such as As-Sc, $r = -0.58$, and As-Ta = -0.95 , may indicate that As is more mobile than Sc and Ta. Both the oxidation of arsenite, As(III), to arsenate, As(V), and the reduction of arsenate to arsenite can be mediated by microorganisms [33–35]. The elevated As content (up to 960 mg/kg) in yellow-whitish, deep red to deep-grey color bauxite samples compared to brown-red samples (average 10 mg/kg As) (Table 1; Figure 5), the elevated total organic carbon (TOC) content (up to 5.4 wt.%) compared to the brown-red ore (0.08–0.26 wt.%), and the positive trend between As and TOC ($r = 0.46$) suggest that the As speciation is controlled by the presence of microorganisms. The creation of an acidic environment during meta-diagenesis stages, due to the decomposition of organic matter, may be responsible for the mobility and the elevated As contents, as well as for the potential presence of arsenate in association with goethite [11]. The investigation by synchrotron radiation (SR) spectroscopic techniques (SR μ -XRF and As K-edge μ -XAFS) of bauxite Fe-Ni-laterite ore from the Lokris area, C. Greece, having significant contents of As and TOC, has shown that As occurs in the form of arsenate anions As(V) or (AsO_4^{3-}) in association with goethite as well [36]. Besides, a positive correlation ($r > 0.50$) between As and Pd, Sb (Table 2) may suggest the potential existence of (As, Pd, Sb)-bearing epigenetic minerals.

The lower PGE content in the Parnassos-Ghiona bauxite ores ranging from <0.1 to $1.9 \mu\text{g/kg Pt}$ and <0.5 to $5.5 \mu\text{g/kg Pd}$ (Table 1), compared to those in Fe-Ni \pm Co laterites reaching up to $88 \mu\text{g/kg Pt}$ and $45 \mu\text{g/kg Pd}$ [37], is similar to that in other bauxite deposits and occurrences [38]. Such a difference may be related to their main parent rocks, as their contribution is reflected in the main components of ophiolites, such as Cr, Ni, and Co [21,38,39]. The relatively high values of the Pd/Pt ratio, ranging from 1.0 to 5.5 in the bauxite profile (Table 1), may be related to the higher solubility and mobility of Pd compared to that of Pt [40]. In addition, such higher Pd/Pt values in karst-type bauxites, compared to the Fe-Ni laterite deposits from the Balkan Peninsula (0.1 to 0.68, average = 0.40), may reflect a Pd-Pt decoupling during the transportation and redeposition at a longer distance from the former than the Fe-Ni laterites, lying on peridotites [37]. Scanning electron microscopy images showing biofilms containing abundant PGE nanoparticles and microcrystalline aggregates have shown that microorganisms can influence the mobility of PGE [41]. These authors described PGE minerals containing C, N, S, Se, and I, suggesting their biogenic origin, and concluded that biofilms are capable of forming or transforming PGE minerals, while secondary PGE minerals have been described at the border of Fe oxide(s) grains elsewhere [42]. Therefore, the Pd and Pt along the bauxite profile (Figure 4) seems to be the result of their solubility and redeposition, facilitated by the interaction with the organic matter during the bauxite origin and redeposition by epigenetic processes.

6.2. Mining/Smelting Processes and Environmental Implications

It is well known that smelting or pyrometallurgy is the traditional technique for Al extraction, but this process is energy-consuming and generates greenhouse gas emissions and metallurgical residue, or red mud, which is relatively toxic. The biogeochemical cycling of metals and metalloids during open-pit mining of bauxite and the large volume of smelting residues may cause change in the land use for large land zones, environmental hazards for terrestrial and aquatic ecosystems, and food quality and socioeconomic problems. Besides

the emissions, due to the metallurgical process of bauxite, the metallurgical residue, or red mud, is relatively toxic due to its high alkalinity (pH 10–12.5) and the presence of heavy and radioactive metals (Cr, V, Cd, Ni, Zn, Pb, REE, U, and Th) [43,44].

Since soils provide plants with certain trace elements in small amounts, which are considered to be critical for the healthy growth of humans, the protection and increase of the soil organic carbon is a priority in the European Union (EU) [9]. The spatial and temporal exploration of the composition and dynamics of bacterial and fungal communities in bauxite residues [45] has revealed that both deposit age and ore origin affect the geochemistry of bauxite residue. These authors concluded that salinity, pH and TOC depend predominantly on the age of bauxite residue, while the content of REE is mainly influenced by the origin of the bauxite ore. In addition, the investigation of the fertility of natural forest soil affected by the bauxite mining activities in Indonesia revealed that the fertility decreases for total N, C and P contents, exchangeable Ca, Mg and Na contents, and the growth of tree species [46]. Fertilizers and microorganisms have been applied to improve the soil fertility of post-open-pit mining land and develop bioindicators for the remediation of land contaminated by the mining of bauxite [47]. The soil biogeochemistry and arsenic mobility in soil-water has been investigated experimentally using As-bearing red mud from Ajka (Hungary) and it was found that As was present as arsenate, As(V), which is highly pH-dependent, while the addition of phosphate to red mud greatly enhanced As release to solution [48]. In addition, investigation of the area contaminated by red mud Ajka (Hungary) showed that trace element contents, such as Cu, Cr, Ni, B, and Fe in plant shoots increased significantly with increasing dose of red mud, but none of these exceeded toxic limits, and Na salinity should be the main concern for this red mud in soil [49].

In general, the accumulation of multi-oxidation-state elements or transfer factor, e.g., the ratio of the element content in plants relative to the total element content in the corresponding soil, depends on the amount of elements in the soil and their mobility, the physical/chemical parameters (pH, Eh), the concentrations of competing ions, organic matter content, and other parameters [50]. An integrated approach to the soil, plant crops, and groundwater system has been performed to several cultivated basins with potential contamination, to evaluate the bioaccumulation of toxic elements by plants, a potential threat for human health and ecosystems [51]. However, water leachates for red mud from the Aspra Spitia plant have shown unexpectedly high (2100 µg/LCr(VI)) concentrations [23], suggesting the potential contamination of neighboring soil and groundwater. Microbe-mediated mineralization has important applications in the restriction and/or removal of contaminants, such as the potential transfer of Cr(VI) in cultivated basins from area contaminated by red mud. The toxic hexavalent chromium [(Cr(VI))] in the food chain has created an alarming situation for human life and ecosystems, and the ability of organic matter (leonardite) in reducing Cr uptake by crops for soil and irrigation water with Cr(VI) has been investigated [52]. These authors concluded that the highest Cr values in shoots and in roots were recorded in those plants cultivated in soil after the addition of Cr(VI)-water without organic matter, and the lowest Cr values were in shoots and in roots of plants cultivated in soil with addition of 30 wt.% organic matter. Thus, the organic matter may provide a cost-effective method for the restriction of Cr transfer from contaminated soils and irrigation water to plants/crops and contribute to the better management of soil and water use.

7. Conclusions

Mineral transformations and compositional variations along a bauxite profile underlying a fault at the Parnassos-Ghiona deposit, Greece, point to the following conclusions:

- Multicolor ores: grey-whitish (top), yellowish, deep red, and deep grey to brown-red color (bottom) are all associated with fossilized and present-day microorganisms, with TOC content showing the highest values in the deep grey ores and the lowest in the brown-red ores.

- The recorded compositional variations show that the Al enrichment is accompanied by an increase in the TOC, As, Pd, and U, while the chondrite-normalized REE patterns through the whole profile exhibit a similar trend and positive Ce anomalies.
- The lower (Pt + Pd) content and Pd/Pt ratio higher in the bauxite profile, compared to those in Fe-Ni laterite deposits, may reflect the higher solubility and mobility of Pd compared to that of Pt, and differences in their origin and genesis.
- A positive correlation between Pd and As and the elevated As content (up to 960 mg/kg) in multicolor ores compared to brown-red samples (average 10 mg/kg As) point to their mobilization and epigenetic enrichment.
- Geochemical characteristics of bauxite ores and smelting residues and their water leachates suggest that cycling of metals and metalloids during open-pit mining of bauxite and the large volume of red mud may cause changes to the land use, ecosystems, and the food quality.
- Microorganisms, by their reducing and/or oxidizing activity, catalyze redox reactions, resulting in the Fe(II) migration and precipitation of framboidal pyrite as veins crosscutting previous phases, and provide nucleation sites for the precipitation of secondary minerals.

Author Contributions: Conceptualization and methodology: M.E.-E., M.K. and I.M.; software and validation of data: M.K. and I.M.; writing—original draft preparation: M.E.-E. and I.M. All authors have read and agreed to the published version of the manuscript.

Funding: This research was funded by the University of Athens (Grant No KE 11078).

Data Availability Statement: Not applicable.

Acknowledgments: Many thanks are expressed once again to the University of Athens for the financial support and George Tsoupas for his assistance with the collection of the bauxite samples. The criticism and constructive suggestions by the anonymous reviewers are very much appreciated.

Conflicts of Interest: The authors declare no conflict of interest.

References

1. Gadd, M.G. Metals, minerals and microbes: Geomicrobiology and bioremediation. *Microbiology* **2010**, *156*, 609–643. [[CrossRef](#)] [[PubMed](#)]
2. Gupta, A.; Ehrlich, H.L. Selective and non-selective bioleaching of manganese containing silver ore. *J. Biotechnol.* **1989**, *9*, 287–304. [[CrossRef](#)]
3. Banfield, J.F.; Nealson, K.H. (Eds.) *Geomicrobiology: Interactions between Microbes and Minerals, Reviews in Mineralogy and Geochemistry*; Mineralogical Society of America: Washington, DC, USA, 1997; Volume 35.
4. Berthelin, J. Microbial Weathering Processes in Natural Environments. In *Physical and Chemical Weathering in Geochemical Cycles*; NATO ASI Series (Series C: Mathematical and Physical Sciences); Lerman, A., Meybeck, M., Eds.; Springer: Dordrecht, The Netherlands, 1988; Volume 251, pp. 33–59. [[CrossRef](#)]
5. Cassard, D.; Bertrand, G.; Billa, M.; Serrano, J.J.; Tourlière, B.; Angel, J.M.; Gaál, G. ProMine Mineral Databases: New Tools to Assess Primary and Secondary Mineral Resources in Europe. In *3D, 4D and Predictive Modelling of Major Mineral Belts in Europe*; Weihed, P., Ed.; Springer: Cham, Switzerland, 2015.
6. European Commission. *Critical Raw Materials Resilience: Charting a Path towards Greater Security and Sustainability. Communication from the Commission to the European Parliament, the Council, the European Economic and Social Committee 2 and the Committee of the Regions COM(2020) 474 Final*; European Commission: Brussels, Belgium, 2020.
7. Dixit, R.; Malaviya, D.; Pandiyan, K.; Singh, U.B.; Sahu, A.; Shukla, R.; Singh, B.P.; Rai, J.P.; Sharma, P.K.; Lade, H. Bioremediation of heavy metals from soil and aquatic environment: An overview of principles and criteria of fundamental processes. *Sustainability* **2015**, *7*, 2189–2212. [[CrossRef](#)]
8. Mohanty, S.P.; Hughes, D.P.; Salathé, M. Using deep learning for image-based plant disease detection. *Front. Plant Sci.* **2016**, *7*, 1419. [[CrossRef](#)] [[PubMed](#)]
9. Van der Putten, W.; Poesen, J.; Lisá, L.; Winding, A.; Moora, M.; Lemanceau, P.; Setälä, H.; Zaitsev, A.; Economou-Eliopoulos, M.; Hornung, E.; et al. *Opportunities for Soil Sustainability in Europe*; European Academies' Science Advisory Council: Halle, Germany, 2018; p. 41.
10. Laskou, M.; Economou-Eliopoulos, M. The role of microorganisms on the mineralogical and geochemical characteristics of the Parnassos-Ghiona bauxite deposits, Greece. *J. Geochem. Explor.* **2007**, *93*, 67–77. [[CrossRef](#)]

11. Laskou, M.; Economou-Eliopoulos, M. Bio-mineralization and potential biogeochemical processes in bauxite deposits: Genetic and ore quality significance. *Miner. Petrol.* **2013**, *407*, 171–186. [[CrossRef](#)]
12. Kontou, M. Iron Bio-Leaching of Bauxites. Ph.D. Thesis, National and Kapodistrian University of Athens, Athens, Greece, 2009; p. 141.
13. Kalaitzidis, S.; Siavalas, G.; Skarpelis, N.; Araujo, C.V.; Christanis, C. Late Cretaceous coal overlying karstic bauxite deposits in the Parnassos-Ghiona Unit, Central Greece: Coal characteristics and depositional environment. *Int. J. Coal Geol.* **2010**, *81*, 211–226. [[CrossRef](#)]
14. Gamaletsos, P. Mineralogy and Geochemistry of Bauxites from Parnassos-Ghiona Mines and the Impact on the Origin of the Deposits. Ph.D. Thesis, National and Kapodistrian University of Athens, Athens, Greece, 2014; p. 347.
15. Combes, P.-J. Regards sur la géologie des bauxites; aspects récents sur la genèse de quelques gisements à substratum carbonate—A look at the geology of bauxite; recent data on the genesis of some deposits in carbonate rock. *Bulletin des Centres de Recherches Exploration—Production Elf-Aquitaine* **1984**, *8*, 251–274.
16. Radusinović, S.; Papadopoulos, A. The Potential for REE and Associated Critical Metals in Karstic Bauxites and Bauxite Residue of Montenegro. *Minerals* **2021**, *11*, 975. [[CrossRef](#)]
17. Abedini, A.; Mehr, M.H.; Khosravi, M.; Calagari, A.A. Geochemical characteristics of the karst-type bauxites: An example from the Kanirash deposit, NW Iran. *Arab. J. Geosci.* **2019**, *12*, 1–16. [[CrossRef](#)]
18. Laskou, M. Pyrite-rich bauxites from the Parnassos-Ghiona zone, Greece. In *Mineral Deposit Research: Meeting the Global Challenge*; Mao, J., Bierlein, F.P., Eds.; Springer: Berlin/Heidelberg, Germany, 2005; pp. 1007–1010.
19. Laskou, M.; Economou-Eliopoulos, M.; Mitsis, I. Biomineralization of halotrichite and sulphates on bauxite ores. In Proceedings of the Goldschmidt 2010 Conference, Knoxville, TN, USA, 13–18 June 2010; p. A564.
20. Walkley, A.; Black, L.A. An examination of the Dgtjareff method for determining soil organic matter, and a proposed modification of the chromic acid titration method. *Soil Sci.* **1934**, *37*, 29–38. [[CrossRef](#)]
21. Valetou, I.; Bierman, M.; Reche, R.; Rosenberg, F.F. Genesis of nickel laterites and bauxites in Greece during the Jurassic and the Cretaceous and their relation to ultrabasic rocks. *Ore Geol. Rev.* **1987**, *2*, 359–404. [[CrossRef](#)]
22. Williams, R.J. Karst-associated bauxite deposits of Parnassos-Ghiona, Central Greece: Ore Genesis and Structural Evolution. Ph.D. Thesis, University of Brighton, Brighton, UK, June 2014.
23. Economou-Eliopoulos, M.; Frei, R.; Megremi, I. Potential leaching of Cr(VI) from laterite mines and residues of metallurgical products (red mud and slag): An integrated approach. *J. Geochem. Explor.* **2016**, *262*, 40–49. [[CrossRef](#)]
24. Russell, M.J.; Hall, A.J.; Boyce, A.J.; Fallick, A.E. 100th Anniversary special paper: On hydrothermal convection systems and the emergence of life. *Econ. Geol.* **2005**, *100*, 419–438.
25. Falkowski, P.G.; Fenchel, T.; Delong, E.F. The microbial engines that drive earth's biogeochemical cycles. *Science* **2008**, *320*, 1034–1039. [[CrossRef](#)] [[PubMed](#)]
26. Ehrlich, H.; Witkowski, A. Biomineralization in Diatoms: The Organic Templates. In *Evolution of Lightweight Structures. Biologically-Inspired Systems*; Hamm, C., Ed.; Springer: Dordrecht, The Netherlands, 2015; Volume 6. [[CrossRef](#)]
27. Fischer, A.; Schmitz, M.; Aichmayer, B.; Fratzl, P.; Faivre, D. Structural purity of magnetite nanoparticles in magnetotactic bacteria. *J. R. Soc. Interface* **2011**, *8*, 1011–1018. [[CrossRef](#)]
28. Polgári, M.; Gyollai, I. Geochemical constraints on the element enrichments of microbially mediated manganese and iron ores—An overview. *Ore Geol. Rev.* **2021**, *136*, 104203. [[CrossRef](#)]
29. Baskar, S.; Baskar, R.; Kaushik, A. Role of microorganisms in weathering of the Konkan-Goa laterite formation. *Curr. Sci.* **2003**, *85*, 1129–1134.
30. Southam, G.; Saunders, J. The geomicrobiology of ore deposits. *Econ. Geol.* **2005**, *100*, 1067–1084. [[CrossRef](#)]
31. Timotijević, S. *Cretaceous Bauxites of Serbia*; Special Editions of the Geo Institute No. 27; Geological Survey of Serbia: Belgrade, Serbia, 2001; pp. 1–183.
32. Yalcin, M.G.; Ilhan, S. Major and Trace Element Geochemistry of Bauxites of Ayranci, Karaman, Central Bolcardag, Turkey. *Asian J. Chem.* **2013**, *25*, 2893–2904. [[CrossRef](#)]
33. Huang, J.H. Impact of Microorganisms on Arsenic Biogeochemistry: A Review. *Water Air Soil Pollut.* **2014**, *225*, 1848. [[CrossRef](#)]
34. Campbell, B.J.; Engel, A.S.; Porter, M.L.; Takai, K. The versatile epsilon-proteobacteria: Key players in sulphidic habitats. *Nat. Rev. Microbiol.* **2006**, *4*, 458–468. [[CrossRef](#)] [[PubMed](#)]
35. Chen, C.; Li, L.; Huang, K. Sulfate-reducing bacteria and methanogens are involved in arsenic methylation and demethylation in paddy soils. *ISME J.* **2019**, *13*, 2523–2535. [[CrossRef](#)]
36. Gamaletsos, P.N.; Kalatha, S.; Godelitsas, A.; Economou-Eliopoulos, M.; Göttlicher, J.; Steininger, R. Arsenic distribution and speciation in the bauxitic Fe-Ni-laterite ore deposit of the Patitira mine, Lokris area (Greece). *J. Geochem. Explor.* **2018**, *194*, 189–197. [[CrossRef](#)]
37. Economou-Eliopoulos, M.; Laskou, M.; Eliopoulos, D.G.; Megremi, I.; Kalatha, S.; Eliopoulos, G.D. Origin of Critical Metals in Fe-Ni Laterites from the Balkan Peninsula: Opportunities and Environmental Risk. *Minerals* **2021**, *11*, 1009. [[CrossRef](#)]
38. Laskou, M.; Economou, M. Palladium, Pt, Rh and Au Contents in Some Bauxite Occurrences of Greece. In Proceedings of the Balkan-Carpathian Congress, Sofia, Bulgaria, 11–13 December 1989; pp. 1367–1371.
39. Eliopoulos, D.G.; Economou-Eliopoulos, M. Geochemical and mineralogical characteristics of Fe-Ni and bauxitic-laterite deposits of Greece. *Ore Geol. Rev.* **2000**, *16*, 41–58. [[CrossRef](#)]

40. Grey, J.D.; Schorin, K.H.; Butt, C.R.M. Mineral associations of platinum and palladium in lateritic regolith, Ora Banda Sill, Western Australia. *J. Geochem. Explor.* **1996**, *57*, 245–255. [[CrossRef](#)]
41. Reith, F.; Zammit, C.M.; Shar, S.S.; Etschmann, B.; Bottrill, R.; Southam, G.; Ta, C.; Kilburn, M.; Oberthür, T.; Ball, A.S.; et al. Biological role in the transformation of platinum-group mineral grains. *Nat. Geosci.* **2016**, *9*, 294–298. [[CrossRef](#)]
42. Aiglsperger, T.; Proenza, J.A.; Lewis, J.F.; Labrador, M.; Svojtka, M.; Rojas-Purón, A.; Longo, F.; Ďurišová, J. Critical metals (REE, Sc, PGE) in Ni laterites from Cuba and the Dominican Republic. *Ore Geol. Rev.* **2016**, *73*, 127–147. [[CrossRef](#)]
43. Kumar, M. An approach towards green alumina refinery and sustainable development. *Travaux* **2011**, *36*, 11–22.
44. Gamaletsos, P.N.; Godelitsas, A.; Filippidis, A.; Pontikes, Y. The Rare Earth Elements Potential of Greek Bauxite Active Mines in the Light of a Sustainable REE Demand. *J. Sustain. Met.* **2018**, *5*, 20–47. [[CrossRef](#)]
45. Macías-Pérez, L.A.; Levard, C.; Barakat, M.; Angeletti, B.; Borschnek, D. Contrasted microbial community colonization of a bauxite residue deposit marked by a complex geochemical context. *J. Hazard. Mater.* **2022**, *424*, 127470. [[CrossRef](#)]
46. Prematuri, R.; Turjaman, M.; Sato, T.; Tawaraya, K. Post Bauxite Mining Land Soil Characteristics and Its Effects on the Growth of *Falcataria moluccana* (Miq.) Barneby & J. W. Grimes and *Albizia saman* (Jacq.). *Merr. Appl. Environ. Soil Sci.* **2020**, *2020*, 6764380. [[CrossRef](#)]
47. Huang, L.; Baumgartl, T.; Mulligan, D. Is rhizosphere remediation sufficient for sustainable revegetation of mine tailings? *Ann. Bot.* **2012**, *110*, 223–238. [[CrossRef](#)]
48. Lockwood, L.C.; Mortimer, J.G.R.; Stewart, I.D.; Mayes, M.W.; Peacock, L.C.; Polya, A.D.; Lythgoe, R.P.; Lehoux, P.A.; Gruiz, K.; Burke, T.I. Mobilisation of arsenic from bauxite residue (red mud) affected soils: Effect of pH and redox conditions. *Appl. Geochem.* **2014**, *51*, 268–277. [[CrossRef](#)]
49. Ruyters, S.; Mertens, J.; Vassilieva, E.; Dehandschutter, B.; Poffijn, A.; Smolders, E. The red mud accident in Ajka (Hungary): Plant toxicity and trace metal bioavailability in red mud contaminated soil. *Environ. Sci. Technol.* **2010**, *45*, 1616–1622. [[CrossRef](#)]
50. Liesack, W.; Schnell, S.; Revsbech, N.P. Microbiology of flooded rice paddies. *FEMS Microbiol. Rev.* **2000**, *24*, 624–645. [[CrossRef](#)] [[PubMed](#)]
51. Megremi, I.; Vasilatos, C.; Vassilakis, E.; Economou-Eliopoulos, M. Spatial diversity of Cr distribution in soil and groundwater sites in relation with land use management in a Mediterranean region: The case of C. Evia and Assopos-Thiva Basins, Greece. *Sci. Total Environ.* **2019**, *651*, 656–667. [[CrossRef](#)] [[PubMed](#)]
52. Raptis, S.; Gasparatos, D.; Economou-Eliopoulos, M.; Petridis, A. Chromium uptake by lettuce as affected by the application of organic matter and Cr (VI)-irrigation water: Implications to the land use and water management. *Chemosphere* **2018**, *210*, 597–606. [[CrossRef](#)] [[PubMed](#)]